DMD Fast Forward. Published on February 13, 2022 as DOI: 10.1124/dmd.121.000804
This article has not been copyedited and formatted. The final version may differ from this version.

Direct and Sequential Bioactivation of Pemigatinib to Reactive Iminium Ion Intermediates Culminate in Mechanism-Based Inactivation of Cytochrome P450 3A

Lloyd Wei Tat Tang[1#], Wan Wei[2#], Ravi Kumar Verma[2], Siew Kwan Koh[3], Lei Zhou[3,4,5], Hao Fan[2] and Eric Chun Yong Chan[1]

[1]Department of Pharmacy, Faculty of Science, National University of Singapore, Singapore

[2]Bioinformatics Institute (BII), Agency for Science, Technology and Research (A*STAR), Singapore

[3]Singapore Eye Research Institute (SERI), Singapore

[4]Department of Ophthalmology, Yong Loo Lin School of Medicine, National University of Singapore, Singapore

[5]Ophthalmology and Visual Sciences Academia Clinical Program, Duke-National University of Singapore Medical School, Singapore

[#]*L.W.T.T and W.W contributed equally to the work.*

DMD Fast Forward. Published on February 13, 2022 as DOI: 10.1124/dmd.121.000804
This article has not been copyedited and formatted. The final version may differ from this version.

Running Title:

Mechanism-Based Inactivation of CYP3A by Pemigatinib

Address Correspondence to:

Professor Eric Chun Yong Chan, Department of Pharmacy, National University of Singapore, 18 Science Drive 4, Singapore 117543.

Email: phaccye@nus.edu.sg; Telephone: +65-6516 6137; Fax: +65-6779 1554

Number of Tables	4
Number of Figures	11
Number of References	44
Number of words in the Abstract	234
Number of words in the Significance Statement	77
Number of words in the Introduction	748
Number of words in the Discussion	1500

DMD Fast Forward. Published on February 13, 2022 as DOI: 10.1124/dmd.121.000804
This article has not been copyedited and formatted. The final version may differ from this version.

ABBREVIATIONS

CYP3A4	Cytochrome P450 3A4
CYP3A5	Cytochrome P450 3A5
DDI	Drug-drug interaction
FDA	United States Food and Drug Administration
FGFR	Fibroblast growth factor receptor
GSH	Glutathione
G6P	Glucose-6-phosphate
G6PDH	Glucose-6-phosphate dehydrogenase
HPLC	High-performance liquid chromatography
KCN	Potassium cyanide
K_I	Inactivator concentration at half-maximum inactivation rate constant
k_{inact}	Maximum inactivation rate constant
K_m	Michaelis constant
k_{obs}	Observed first-order rate constant of inactivation
IADR	Idiosyncratic adverse drug reactions
LC/MS/MS	Liquid chromatography tandem mass spectrometry
MBI	Mechanism-based inactivation
MD	Molecular dynamics
MIC	Metabolite-intermediate complex
MRM	Multiple reaction monitoring
OBS	Orthosteric binding site
P450	Cytochrome P450
rhCYP3A4	Recombinant human cytochrome P450 3A4
rhCYP3A5	Recombinant human cytochrome P450 3A5
ROS	Reactive oxygen species
$t_{1/2}$	Half-life
TDI	Time-dependent inhibition

DMD Fast Forward. Published on February 13, 2022 as DOI: 10.1124/dmd.121.000804
This article has not been copyedited and formatted. The final version may differ from this version.

ABSTRACT

We recently established the mechanism-based inactivation (MBI) of cytochrome P450 3A (CYP3A) by the fibroblast growth factor receptor (FGFR) inhibitors erdafitinib and infigratinib. Serendipitously, our preliminary data has also revealed that pemigatinib (PEM) – another clinically approved FGFR1-3 inhibitor – similarly elicited time-dependent inhibition of CYP3A. This was rather unexpected as it was previously purported that PEM did not pose any metabolism-dependent liabilities due to the absence of glutathione-related conjugates in metabolic profiling experiments conducted in human liver microsomes. Here, we confirmed that PEM inhibited both CYP3A isoforms in a time-, concentration-, and cofactor-dependent manner consistent with MBI – with K_I, k_{inact}, and partition ratio of 8.69 and 11.95 μM, 0.108 and 0.042 min^{-1}, and ~44 and ~47 for CYP3A4 and CYP3A5 respectively. While the rate of inactivation was diminished by coincubation with an alternative substrate or direct inhibitor of CYP3A, the inclusion of nucleophilic trapping agents afforded no such protection. Furthermore, the lack of catalytic activity recovery following dialysis and oxidation with potassium ferricyanide coupled with the absence of a spectrally resolvable peak in the Soret region collectively implied that the underlying mechanism of inactivation was not elicited via the formation of pseudo-irreversible metabolite-intermediate complexes. Finally, utilizing cyanide trapping and high-resolution mass spectrometry, we illuminated the direct and sequential oxidative bioactivation of PEM and its major *O*-desmethylated metabolite at its distal morpholine moiety to reactive iminium ion hard electrophilic species that could covalently mechanism-based inactivate CYP3A.

Keywords: pemigatinib, CYP3A, mechanism-based inactivation, bioactivation, covalent adduction, reactive metabolite

DMD Fast Forward. Published on February 13, 2022 as DOI: 10.1124/dmd.121.000804
This article has not been copyedited and formatted. The final version may differ from this version.

SIGNIFICANCE STATEMENT

In this study, we reported for the first time the covalent MBI of CYP3A by PEM and deciphered its bioactivation pathway involving the metabolic activation of PEM and its major *O*-desmethylated metabolite to reactive iminium ion intermediates. Following which, a unique covalent docking methodology was harnessed to unravel the structural and molecular determinants underpinning its inactivation. Findings from our study lay the foundation for future investigation of clinically-relevant drug-drug interactions between PEM and concomitant substrates of CYP3A.

DMD Fast Forward. Published on February 13, 2022 as DOI: 10.1124/dmd.121.000804
This article has not been copyedited and formatted. The final version may differ from this version.

INTRODUCTION

Multiple lines of evidence have demonstrated that genomic aberrations in fibroblast growth factor receptors (FGFR) (i.e., gene amplification or chromosomal translocations) may result in its constitutive activation and drive oncogenesis or development of resistance to anticancer therapies in several solid tumours (Turner and Grose, 2010; Babina and Turner, 2017). Consequently, pharmacological ablation of FGFR signalling pathways is gaining prominence as a promising treatment modality in oncology (Dienstmann *et al.*, 2014; Ghedini *et al.*, 2018). At present, three FGFR-selective inhibitors are clinically utilized in the armamentarium against FGFR-driven malignancies (Chae *et al.*, 2017; Markham, 2019; Hoy, 2020). One such agent is pemigatinib (PEM) **(Fig. 1A)**, a highly potent and selective inhibitor of FGFR1-3 that has garnered accelerated approval by the U.S Food and Drug Administration (FDA) in 2020 for the treatment of advanced or metastatic cholangiocarcinoma harbouring FGFR2 fusions or rearrangements (Liu *et al.*, 2020).

Previous pharmacokinetic studies have revealed that PEM undergoes extensive hepatic metabolism by cytochrome P450 3A enzymes (CYP3A) – with majority of the dose recovered as the *O*-desmethylated metabolite **(Fig. 1B)** (Ji *et al.*, 2021). Collectively, the cytochrome P450 (P450) superfamily serves as one of the major driving forces of oxidative metabolism in the human body (Guengerich, 2001; Zanger and Schwab, 2013). It is estimated that the metabolism of >80% of all marketed drugs can be ascribed to just six P450 isoforms (Zanger *et al.*, 2008), thereby entrenching their significance in drug disposition. However, due to their wide substrate and catalytic promiscuity, there is broad consensus that P450 could also inadvertently perpetrate metabolic activation of drugs which may result in idiosyncratic adverse drug reactions (IADR) (Guengerich, 2001). Also termed as

bioactivation, the reaction results in the generation of electrophilic, reactive intermediates that – when liberated – may covalently alkylate to nucleophilic centres on biological macromolecules or disrupt cellular redox homeostasis via the production of reactive oxygen species (ROS) (Stephens *et al.*, 2014).

Apart from their potential overt toxicological consequences, the reactive intermediate generated could also be sequestered via covalent adduction to the P450 apoprotein and/or prosthetic heme or through coordination with the heme ferrous which could engender time-dependent inhibition (TDI) of its catalytic activity via mechanism-based inactivation (MBI) (Ho *et al.*, 2015). As the loss of enzymatic activity incited by MBI is irreversible and persists *in vivo* even after the perpetrator drug has been systemically cleared from the body and is only restored upon *de novo* synthesis of the implicated enzyme, the extent of drug-drug interactions (DDI) tends to be more profound than with a direct reversible inhibitor (Bjornsson *et al.*, 2003). Furthermore, covalent modification of the P450 protein may constitute neoantigens and trigger autoimmune reactions leading to immune-mediated toxicities (Masubuchi and Horie, 2007). Due to the manifold ramifications of MBI in pharmacology and toxicology, it becomes clinically important to discern if a drug elicits MBI of P450 – which is in turn characterized by the following salient features: time- and cofactor-dependency of inactivation, saturable kinetics of inactivation, protection against inactivation by a competing substrate, lack of protection by exogenous nucleophiles or scavengers of ROS, irreversibility of inactivation and a 1:1 binding stoichiometry (Silverman, 1995). Notably, our group has recently characterized the MBI and mapped the bioactivation pathways of erdafitinib and infigratinib (two other FDA-approved FGFR inhibitors) by CYP3A (Tang *et al.*, 2021a; Tang *et al.*, 2021b). Intriguingly, our preliminary data has also hinted that PEM similarly elicited such metabolism-dependent inhibition of

DMD Fast Forward. Published on February 13, 2022 as DOI: 10.1124/dmd.121.000804
This article has not been copyedited and formatted. The final version may differ from this version.

CYP3A. This was rather unexpected as it was previously purported by the manufacturer that PEM did not pose any bioactivation-dependent liabilities due to the absence of glutathione (GSH)-related conjugates in reactive metabolite screens conducted in human microsomal fractions (Wu *et al.*, 2021). While the majority of reactive metabolites (i.e. epoxides, quinones, quinone-imines, quinone-methides etc) are soft electrophiles and can be effectively trapped by GSH, electrophilic species arising from the oxidative bioactivation of cyclic tertiary amines or primary alcohols (i.e. iminiums, aldehydes) are less polarizable and can only be trapped by a nucleophile of comparable 'hardness' (Pearson, 1963). Consequently, we posited that PEM is metabolically activated by CYP3A to a hard electrophile, thereby allowing it to elude GSH trapping and detection in the aforementioned metabolic profiling assay.

In this study, we revealed for the first time that PEM is an archetypal MBI of CYP3A4 and CYP3A5 and further confirmed our postulations through cyanide trapping and high-resolution mass spectrometry that it is liable to be directly and sequentially bioactivated at its distal morpholine moiety to reactive iminium ion intermediates that are likely implicated in the covalent MBI of CYP3A.

DMD Fast Forward. Published on February 13, 2022 as DOI: 10.1124/dmd.121.000804
This article has not been copyedited and formatted. The final version may differ from this version.

MATERIALS AND METHODS

Chemicals and Reagents. PEM and erdafitinib were procured from MedChem Express (Monmouth Junction, NJ). Potassium ferricyanide was obtained from VWR International (Leuven, Belgium). Dexamethasone, ketoconazole, potassium cyanide (KCN), rivaroxaban, GSH and catalase were acquired from Sigma-Aldrich (St. Louis, MO). Human recombinant P450 3A4 and 3A5 Supersomes (rhCYP3A4 and rhCYP3A5) co-expressing cytochrome b_5 and NADPH P450 reductase and the NADPH regenerating system comprising NADP+ and glucose-6-phosphate (G6P) (NADPH A) and glucose-6-phosphate dehydrogenase (G6PDH) (NADPH B) were commercially purchased from Corning Gentest (Woburn, MA). High performance liquid chromatography (HPLC)-grade acetonitrile was procured from Tedia Company Inc. (Fairfield, OH). Ultrapure water (type I) was prepared in-house using a Milli-Q water purification system (Millipore Corporation, Bedford, MA). All other commercially available chemicals were of analytical or HPLC-grade.

Substrate Depletion of PEM by CYP3A4 and CYP3A5. Unless otherwise stated, all incubations described in this work were performed in 96-well plates. Incubation mixtures comprising 20 pmol/mL rhCYP3A4/5, 1 µM PEM, G6PDH and 100 mM potassium phosphate buffer (pH 7.4) were prepared in triplicates. After pre-warming at 37°C for 5 min, the reaction was initiated via the addition of NADP+/G6P. The final primary incubation mixture (100 µL) contained <1% v/v organic solvent. Subsequently, at various time intervals (0, 5, 12.5, 30, 45, 60, 80 and 100 min), an 80 µL aliquot of each incubation mixture was withdrawn and quenched with equal volumes of ice-cold acetonitrile spiked with internal standard (0.1 µM erdafitinib). The quenched samples were then centrifuged at 4000*g* at 4°C for 30 min, thereafter

DMD Fast Forward. Published on February 13, 2022 as DOI: 10.1124/dmd.121.000804
This article has not been copyedited and formatted. The final version may differ from this version.

aliquots of the supernatant were withdrawn to quantify the amount of PEM remaining using liquid chromatography-tandem mass spectrometry (LC/MS/MS).

Time-, Concentration-, and NADPH-dependent Inactivation of CYP3A. Enzyme inactivation kinetic assays were previously optimized and performed as outlined in our recent works using rivaroxaban as clinically-relevant probe substrate of CYP3A (Tang *et al.*, 2021a; Tang *et al.*, 2021b). Briefly, primary incubation mixtures comprising 40 pmol/mL rhCYP3A4/5, PEM (0, 1, 2.5, 5, 15, and 25 µM), G6PDH and 100 mM potassium phosphate buffer (pH 7.4) were prepared in triplicates. After preincubating at 37°C for 5 min, the reaction was initiated via the addition of NADP+/G6P. The final primary incubation mixture (100 µL) contained <1% v/v organic solvent. Subsequently, at various preincubation intervals (0, 3, 8, 15, 22 and 30 min), a 5 µL aliquot of each primary incubation mixture was withdrawn and diluted 20-fold into a pre-warmed secondary incubation mixture comprising 50 µM rivaroxaban (~4× K_m), an NADPH regenerating system (1 mM) and 100 mM potassium phosphate buffer (pH 7.4). The secondary incubation mixtures were then further incubated at 37°C for an additional or 2 h. After which, an 80 µL aliquot was immediately withdrawn and quenched with equal volumes of ice-cold acetonitrile spiked with internal standard (4 µM dexamethasone). The quenched samples were centrifuged at 4000*g* at 4°C for 30 min to obtain the supernatant for LC/MS/MS analysis. Negative control experiments were performed by substituting NADP+/G6P with 100 mM potassium phosphate buffer (pH 7.4).

Calculation of MBI Kinetic Parameters (K_I and k_{inact}). To derive the inactivation kinetic parameters (K_I and k_{inact}), the mean of triplicate peak area ratios was used to calculate the natural logarithm of percentage residual P450 enzyme activity

DMD Fast Forward. Published on February 13, 2022 as DOI: 10.1124/dmd.121.000804
This article has not been copyedited and formatted. The final version may differ from this version.

normalized to vehicle which was then plotted against preincubation time for each PEM concentration. The resulting data points were fitted to linear regression and the observed first-order inactivation rate constant (k_{obs}) was derived from the slope of the initial linear decline in CYP3A activity for each PEM concentration. Following which, a plot of k_{obs} against PEM concentrations [*I*] allowed the fitting of inactivation kinetic parameters (K_I and k_{inact}) to non-linear least square regression based on **Equation 1** in GraphPad 8.0.2 (San Diego, CA)

$$k_{\mathrm{obs}} = \frac{k_{\mathrm{inact}} \times [I]}{K_{\mathrm{I}} + [I]} \quad (1)$$

where k_{inact} represents the maximal inactivation rate constant; K_I is the concentration of the inactivator at half-maximum inactivation rate constant and [*I*] is the *in vitro* concentration of PEM. **Equation 1** assumes that there is negligible change of [*I*] during the incubation period and that the loss of enzyme activity purely commensurate with inactivation by PEM. The ratio of k_{inact} to K_I was determined by dividing the mean values of k_{inact} by K_I. Lastly, the time required for half of the enzyme molecules to be inactivated ($t_{1/2}$) was determined by **Equation 2**.

$$t_{1/2} = \frac{ln2}{k_{\mathrm{inact}}} \quad (2)$$

Partition Ratio. Primary incubation mixtures consisting of 100 pmol/mL rhCYP3A4/5, PEM (0, 1, 2.5, 5, 15 and 25 µM), G6PDH and 100 mM potassium phosphate buffer (pH 7.4) were prepared in triplicates. After pre-warming the mixture at 37°C for 5 min, the reaction was initiated via the addition of NADP+/G6P and incubated for 45 min to allow inactivation to go into completion. The final primary incubation mixture (50 µL) contained <1% v/v organic solvent. Thereafter, aliquots of

DMD Fast Forward. Published on February 13, 2022 as DOI: 10.1124/dmd.121.000804
This article has not been copyedited and formatted. The final version may differ from this version.

the primary incubation mixture were withdrawn and transferred to the secondary incubation mixture (similar to that prepared for the inactivation experiments) and incubated at 37°C for another 2 h. Samples were then quenched, centrifuged and assayed for residual enzyme activity as described above. The partition ratio was determined as described in our previous study (Tang *et al.*, 2021c). Briefly, the percentage of residual CYP3A activity was plotted against the molar ratio of PEM to CYP3A4/5 concentration. The turnover number (partition ratio + 1) was obtained by extrapolating the intercept of the linear regression line plotted at lower ratios with the straight line plotted at higher ratios to the abscissa. Finally, the partition ratio was back calculated by subtracting the turnover number by 1.

Substrate Protection. To investigate if enzyme inactivation could be amenable to substrate protection, testosterone (an alternative CYP3A substrate) at a concentration of 100 and 200 μM (equivalent to 1:4 and 1:8 molar ratio of PEM:testosterone) or ketoconazole (a potent reversible inhibitor of CYP3A) at a concentration of 0.1 and 1 μM (corresponding to ~1× and ~10× its K_i value), was introduced separately in triplicates to the primary incubation mixture comprising 40 pmol/mL rhCYP3A4/5, 25 μM PEM, G6PDH and 100 mM potassium phosphate buffer (pH 7.4). The enzymatic reaction was initiated by the addition of NADP+/G6P after pre-warming at 37°C for 5 min. Aliquots were withdrawn at different preincubation time points (0, 3, 8 and 15 min), transferred to the secondary incubation mixture and subsequently quenched, centrifuged and assayed for residual CYP3A enzymatic activity as described above. Primary incubation mixtures that obviated the addition of either testosterone, ketoconazole or both PEM and testosterone or ketoconazole served as the negative controls.

DMD Fast Forward. Published on February 13, 2022 as DOI: 10.1124/dmd.121.000804
This article has not been copyedited and formatted. The final version may differ from this version.

Effect of Exogenous Nucleophile and Scavenger of ROS on Inactivation. Primary incubation mixture containing 40 pmol/mL rhCYP3A4/5, 25 μM PEM, G6PDH and 100 mM potassium phosphate buffer (pH 7.4) were individually fortified with GSH (2 mM) or KCN (1 mM). After preincubating at 37°C for 5 min, the enzymatic reaction was initiated via the addition of NADP+/G6P. At specific preincubation time points (0, 3, 8 and 15 min), aliquots were transferred to the secondary incubation mixtures and subsequently quenched, centrifuged and assayed for residual CYP3A enzymatic activity as described above. Negative controls were prepared without both PEM and GSH/KCN or only without GSH/KCN in the primary incubation mixture. Furthermore, parallel experiments involving the incorporation of catalase (800 U/mL) in place of the exogenous nucleophiles were also performed to investigate the specific effects of scavenger of ROS on the inactivation of CYP3A.

Reversibility of Inactivation. The reversibility of CYP3A inactivation was interrogated by two distinct yet complementary approaches; namely equilibrium dialysis and oxidation by potassium ferricyanide, as described in detail in our previous works (Tang *et al.*, 2021a; Tang *et al.*, 2021b). In the dialysis experiments, triplicate primary incubation mixtures comprising 40 pmol/mL rhCYP3A4/5, 25 μM PEM, G6PDH and 100 mM potassium phosphate buffer (pH 7.4) were preincubated at 37°C for 5 min. Enzymatic reaction was initiated by the addition of NADP+/G6P and allowed to proceed for 30 min. After which, a 5 μL aliquot was transferred to 95 μL of the secondary incubation mixture yielding a 20-fold dilution. Concurrently, 90 μL of the remaining primary incubation mixture was transferred to a Slide-A-Lyzer mini dialysis device (0.1 mL, molecular weight cutoff of 10,000; Pierce Chemical Co., Rockford, IL) and placed in a glass beaker filled with 500 mL of ice-cold 100 mM

DMD Fast Forward. Published on February 13, 2022 as DOI: 10.1124/dmd.121.000804
This article has not been copyedited and formatted. The final version may differ from this version.

potassium phosphate buffer (pH 7.4). The buffer system was maintained on ice (4°C) with constant gentle stirring and accompanied by one fresh buffer change at the second hour. After 4 h, 5 µL of the dialyzed mixture was transferred to each pre-warmed secondary incubation well. All secondary mixtures were further incubated at 37°C for 2 h and subsequently assayed for residual CYP3A enzymatic activity as previously described.

In the experiments involving potassium ferricyanide, a series of three sequential incubations were performed. Briefly, the primary incubation comprised 40 pmol/mL rhCYP3A4/5, G6PDH and 100 mM potassium phosphate buffer (pH 7.4) in the presence or absence of 25 µM PEM. Following initiation of the reaction with the addition of NADP+/G6P and incubation at 37°C for either 0 or 30 min, 20 µL of the primary incubation mixture was aliquoted into an equal volume of secondary incubation mixture containing 100 mM potassium phosphate buffer (pH 7.4) with or without 2 mM potassium ferricyanide. The secondary mixtures were then allowed to incubate at 37°C for another 10 min. Thereafter, 10 µL of the mixture was withdrawn and diluted 10-fold into a tertiary incubation mixture containing 50 µM rivaroxaban (probe substrate), an NADPH regenerating system (1 mM) and 100 mM potassium phosphate buffer (pH 7.4). The reaction mixture was further incubated at 37°C for another 2 h and subsequently assayed for residual CYP3A activity as previously described. The percentage of CYP3A metabolic activity remaining after 0 or 30 min incubation with PEM compared to the corresponding controls in the absence of PEM was calculated using **Equation 3** and **4** respectively.

$$\%\ \text{control}_{0\ min} = \frac{v_{\ (0\ \text{min},(+)\ PEM)}}{v_{\ (0\ \text{min},\ (-)\ PEM)}} \times 100 \qquad (3)$$

DMD Fast Forward. Published on February 13, 2022 as DOI: 10.1124/dmd.121.000804
This article has not been copyedited and formatted. The final version may differ from this version.

$$\%\ \text{control}_{30\ min} = \frac{v_{\ (30\ \text{min},(+)\ PEM)}}{v_{\ (30\ \text{min},(-)\ PEM)}} \times 100 \quad (4)$$

where v represents the residual CYP3A activity. Thereafter, % restoration of metabolic activity of CYP3A was derived by subtracting % control$_{30\ min}$ in the presence of potassium ferricyanide with the corresponding values obtained in the absence of potassium ferricyanide.

Spectral Difference Scanning. Incubation mixtures (200 µL) containing 200 pmol/mL rhCYP3A4/5, 25 µM PEM, G6PDH and 100 mM potassium phosphate buffer (pH 7.4) were prepared and pre-warmed at 37°C for 5 min. Thereafter, the enzymatic reaction was initiated via the addition of NADP+/G6P and immediately scanned from 400 to 500 nm at 5 min intervals over a 1 h duration using a Hidex Sense microplate reader (Hidex, Turku, Finland) thermostated at a constant 37°C. The spectral differences were obtained by comparing the UV absorbances between the sample and reference wells which consisted of vehicle in place of PEM. Additionally, the degree of metabolite-intermediate complex (MIC) formation was also quantitatively evaluated by measuring the absorbance difference between 454 and 490 nm with time.

Cyanide Trapping Assay. Incubation mixtures (250 µL) containing 50 pmol/mL rhCYP3A4, 25 µM PEM, G6PDH, 1 mM KCN and 100 mM potassium phosphate buffer (pH 7.4) were prepared and pre-warmed at 37°C for 5 min. The reaction was then initiated via the addition of NADP+/G6P and incubated at 37°C for 1 h. After which, an equal volume of ice-cold acetonitrile was added to quench the reaction. The resulting mixture was centrifuged at 14,000*g* at 4°C for 15 min. Following which, the supernatant was transferred to a new microcentrifuge tube and dried under a

DMD Fast Forward. Published on February 13, 2022 as DOI: 10.1124/dmd.121.000804
This article has not been copyedited and formatted. The final version may differ from this version.

gentle stream of nitrogen gas (TurboVap LV; Caliper Life Science, Hopkinton, MA). The residue was subsequently reconstituted with 60 µL of ACN-water mixture (3:7), vortexed and centrifuged at 14,000*g* at 4°C for 15 min. The resulting supernatant was then carefully removed and transferred to a fresh vial for LC/MS/MS analysis. Samples which omitted the inclusion of PEM in the incubation mixture served as the negative controls.

***In Silico* Protein Structure and Ligand Preparation.** To interrogate the plausible structural and molecular determinants underscoring the observed MBI of CYP3A elicited by PEM and the apparent discrepancies in inactivation potencies between CYP3A4 and CYP3A5, we employed 61 high-resolution crystal structures (<3 Å) of human CYP3A4 retrieved from the RCSB PDB database and 30 structures for human CYP3A5, which consisted of the two reported high-resolution crystal structures and an ensemble of 28 molecular dynamics (MD) simulation frames generated from our previous trajectory clustering analyses (Tang *et al.*, 2021d). For each protein structure obtained, only chain A was considered. All cocrystallized ligands, except for the heme cofactor, were removed from the structure, followed by reverting any mutated amino acid residues back to their wildtype counterparts. Following which, the protein structures were processed with the protein preparation wizard in Maestro (Schrödinger, NY), and the missing residues and loop segments were added to reconstruct the protein. Lastly, hydrogen atoms were added to the structure, and ionization states of titratable groups were determined. Concurrently, three-dimensional coordinates of PEM were obtained from PubChem database (Kim *et al.*, 2019) and multiple conformers of PEM were generated using LigPrep (Schrödinger, NY). The particular conformer with the lowest energy was then selected for covalent docking simulations.

DMD Fast Forward. Published on February 13, 2022 as DOI: 10.1124/dmd.121.000804
This article has not been copyedited and formatted. The final version may differ from this version.

***In Silico* Binding Site Prediction and Covalent Docking.** Firstly, potential ligand-binding pockets for each of the included CYP3A4 and CYP3A5 structures were identified using the site recognition software Sitemap (Schrödinger, NY). As the flexibility of F-F' loop – a critical region of the CYP3A protein oriented directly above the active site – was previously alluded by our studies to be intricately involved in its inactivation, we identified a list of lysine and serine residues in the vicinity of the orthosteric binding site (OBS) encapsulated by the F-F' and C-terminal loops. The docking of PEM was performed in two sequential stages; PEM was first noncovalently docked in the binding pockets containing the accessible lysine and serine residues using GLIDE (Friesner *et al.*, 2004). If noncovalent docking was successful, covalent docking was then performed for the accessible residues within the pocket using CovDock (Zhu *et al.*, 2014) in the Schrödinger suite. The covalent docking scores obtained were then combined, sorted, and ranked for each accessible residue.

Measurement of PEM and Residual P450 Activity by LC/MS/MS. All samples were analysed using the liquid chromatography tandem mass spectrometry (LC/MS/MS) system consisting of an Agilent 1290 Infinity ultra-high pressure liquid chromatography (Agilent Technologies Inc., Santa Clara, CA) bridged with an QTRAP 3500 tandem mass spectrometry (MS/MS) (AB SCIEX, Framingham, MA). Chromatographic separation of PEM and erdafitinib (internal standard) in the substrate depletion assay was achieved with an ACQUITY ultra-performance liquid ethylene bridged hybrid C_{18}, 1.7 µM, 2.2 × 100 mm column (Waters, Milford, MA) while shorter but similar 50 mm C_{18} column was utilized for the chromatographic separation of the rest of the analytes and internal standards described in this work. The aqueous mobile phase (A) was 0.1% formic acid in water, whereas the organic

DMD Fast Forward. Published on February 13, 2022 as DOI: 10.1124/dmd.121.000804
This article has not been copyedited and formatted. The final version may differ from this version.

mobile phase (B) was 0.1% formic acid in acetonitrile. Mobile phases were delivered at a flow rate of 0.5 mL/min. The column and sample temperature were thermostated at 45°C and 4°C respectively. The gradient elution conditions were as follows: linear gradient from 20 to 80% B (0 – 1.20 min), isocratic at 100% B (1.21 – 2.00 min) and isocratic at 20% B (2.01 – 2.50 min). All analytes were detected in positive electrospray ionization (ESI) mode. The source-dependent MS parameters were as follows: ion spray voltage = 5500 V; source temperature = 500°C; curtain gas (CUR) = 25 psi; ion source gas 1 (sheath gas) = 30 psi; ion source gas 2 (drying gas) = 30 psi. The MRM transitions and compound-dependent MS parameters of the analytes are summarized in **Supplemental Table 1**. Chromatographic peak integration was performed using MultiQuant software version 3.0 (Applied Biosystems, Foster City, CA). For all LC/MS/MS analyses, the peak area of the analyte was expressed as a ratio to the peak area of the internal standard.

Detection of Cyano Adducts by LC/MS/MS. Cyano adducts of putative reactive electrophilic intermediate of PEM were analysed using the LC/MS/MS system comprising an Agilent 1290 Infinity ultra-high pressure liquid chromatography (Agilent Technologies Inc., Santa Clara, CA) interfaced with an QTRAP 5500 MS/MS (AB SCIEX, Framingham, MA). Chromatographic separation was achieved on an ACQUITY ultra-performance liquid ethylene bridged hybrid C_{18}, 1.7 µM, 2.2 × 100 mm column (Waters, Milford, MA). The aqueous mobile phase (A) was 0.1% formic acid in water, whereas the organic mobile phase (B) was 0.1% formic acid in acetonitrile. Mobile phases were delivered at a flow rate of 0.35 mL/min. The column and sample temperature were set at 45°C and 4°C respectively. The gradient elution conditions were as follows: isocratic at 10% B (0 – 2.00 min), linear gradient 10 to 70% B (2.01 – 12.00 min), linear gradient 70 to 90% B (12.01 – 14.00 min), isocratic

DMD Fast Forward. Published on February 13, 2022 as DOI: 10.1124/dmd.121.000804
This article has not been copyedited and formatted. The final version may differ from this version.

at 90% B (14.01 – 18.00 min), isocratic at 10% B (18.01 – 20.00 min). An information-dependent acquisition experiment was conducted to detect PEM-derived cyano conjugates via constant neutral loss (NL) scan of 27 Da in positive ESI mode. Enhanced product ion (EPI) scan was prospectively performed for all potential cyano adducts identified. The source-dependent MS parameters utilized were as follows: ion spray voltage = 4500 V; source temperature = 500°C; curtain gas (CUR) = 30 psi; ion source gas 1 (sheath gas) = 50 psi; ion source gas 2 (drying gas) = 50 psi.

Accurate mass measurement of the PEM-derived cyano adducts identified in the cyanide trapping experiments was performed using an ACQUITY ultra-high pressure liquid chromatography (Waters, Milford, MA) coupled to an Orbitrap Exploris 480 MS (Thermo Fisher Scientific, San Jose, CA). Chromatographic separation was achieved on an ACQUITY ultra-performance liquid ethylene bridged hybrid C_{18}, 1.7 µM, 2.2 × 100 mm column (Waters, Milford, MA). The mobile phases, flow rate, temperature and gradient elution conditions were identical to those described earlier in this section. The injection volume was 3 µL and the analytes were ionized by ESI in positive ion mode under the following conditions: sheath gas: 50 arbitrary units; auxiliary gas: 10 arbitrary units; sweep gas: 1 arbitrary unit; S-lens: 50; ion transfer tube temperature: 325 °C; vaporizer temperature: 350 °C, whereas a normalized collision energy of 20% was applied to fragment all ions. The Orbitrap-MS data were acquired and further processed using Xcalibur 4.4 and Freestyle 1.7 software (Thermo Fisher Scientific, San Jose, CA).

DMD Fast Forward. Published on February 13, 2022 as DOI: 10.1124/dmd.121.000804
This article has not been copyedited and formatted. The final version may differ from this version.

RESULTS

Substrate Depletion of PEM in CYP3A4 and CYP3A5. To elucidate any potential TDI of CYP3A by PEM, we first monitored the depletion of PEM over time by CYP3A4 and CYP3A5. Our results demonstrated that while both CYP3A isoforms were capable of metabolizing PEM, CYP3A4 yielded slightly more efficient metabolism with 42.64 ± 4.05 % of PEM remaining after 100 min **(Fig. 2A)** compared to 66.55 ± 2.18 % in CYP3A5 incubations **(Fig. 2B)**. Notably, two distinct phases were observed in the log-transformed substrate depletion profile of PEM for both CYP3A isoforms **(Fig. 2C and D)**. Consequently, two different elimination rate constants (termed k_{fast} and k_{slow} respectively) were calculated for the substrate depletion of PEM by CYP3A4 and CYP3A5. A comparison of the elimination rate constants in the initial portion of incubation revealed that PEM was metabolized ~2.6 times faster by CYP3A4 as compared to CYP3A5 (i.e. $k_{fast,\ CYP3A4}$ = 0.0132 ± 0.0005 min^{-1} compared with $k_{fast,\ CYP3A5}$ = 0.0051 ± 0.0006 min^{-1}). However, after approximately 60 min of incubation there was a dramatic reduction in its rate of metabolism (i.e. $k_{slow,\ CYP3A4}$ = 0.0009 ± 0.0013 min^{-1} and $k_{slow,\ CYP3A5}$ = 0.0005 ± 0.0029 min^{-1}) which alludes to plausible TDI of CYP3A by PEM.

Time-, Concentration-, and NADPH-dependent Inactivation of CYP3A. We then followed-up with a deeper quantitative characterization of its inactivation kinetics using rivaroxaban – a clinically-relevant and moderately sensitive probe substrate of CYP3A. Our findings revealed that PEM inactivated CYP3A4- and CYP3A5-mediated rivaroxaban hydroxylation in a time- and concentration-dependent manner **(Fig. 3A and D)**, with the most profound loss of enzyme activity obtained when 25 µM PEM was preincubated with CYP3A4 for 30 min. As the k_{obs} determined from the

DMD Fast Forward. Published on February 13, 2022 as DOI: 10.1124/dmd.121.000804
This article has not been copyedited and formatted. The final version may differ from this version.

slopes of each of the included concentrations of PEM approached a maximum inactivation rate constant (k_{inact}) **(Fig. 3B and E)**, it denoted that the loss of CYP3A activity elicited by PEM is saturable and exhibited pseudo-first-order kinetics. The inactivation kinetic parameters (K_I and k_{inact}) of PEM derived from the Kitz-Wilson plot (Kitz and Wilson, 1962) were 8.69 ± 1.62 μM and 0.108 ± 0.008 min^{-1} for CYP3A4 and 11.95 ± 4.41 μM and 0.042 ± 0.007 min^{-1} for CYP3A5. This in turn yielded respective k_{inact}/K_I ratios of 12.4 and 3.5 $min^{-1}mM^{-1}$ and inactivation $t_{1/2}$ of 6.4 and 16.5 min. Taken together, our results demonstrated that PEM was a more potent inactivator of CYP3A4 as compared to CYP3A5. All reported values of K_I, k_{inact}, k_{inact}/K_I ratio and $t_{1/2}$ are summarized in **Table 1**. Additionally, as the intentional omission of cofactor NADPH nullified the loss of CYP3A-mediated rivaroxaban hydroxylase activity **(Fig. 3C and E)**, it implied that metabolic activation of PEM was a key molecular-initiating event that preceded the inactivation of CYP3A.

Partition Ratio. A previously described titration method (Silverman, 1995) was adopted, which determined the turnover number for the inactivation of CYP3A4 and CYP3A5 to be ~45 and ~48 respectively **(Fig. 4A and 4B)**. This in turn corresponded to a partition ratio of ~44 and ~47 **(Table 1)**.

Substrate Protection. The **i**nactivation of CYP3A by PEM was protected in the presence of both an alternative substrate and direct inhibitor. Wherein coincubation with either testosterone **(Fig. 5A and D)** or ketoconazole **(Fig. 5B and E)** diminished the rate of inactivation by PEM as evident by the attenuated rate of enzyme inactivation with time. Additionally, the degree of substrate protection appeared to be dose-dependent – with the complete abolishment of inactivation when 1 μM

DMD Fast Forward. Published on February 13, 2022 as DOI: 10.1124/dmd.121.000804
This article has not been copyedited and formatted. The final version may differ from this version.

ketoconazole was coincubated with PEM and CYP3A in the primary incubation mixture.

Effect of Exogenous Nucleophile and Scavenger of ROS on Inactivation. Conversely, the inclusion of nucleophilic trapping agents (i.e. GSH and KCN) and catalase afforded no protection from inactivation. As evident in **Fig. 5C and F**, CYP3A was inactivated to a similar extent in incubation mixtures comprising PEM alone.

Reversibility of Inactivation. To decipher whether the inactivation of CYP3A by PEM is pseudo-irreversible or irreversible, the specific nature of inactivation was interrogated via equilibrium dialysis and oxidation with potassium ferricyanide. Our findings revealed that the magnitude of CYP3A activity was not restored after dialysis at 4°C for 4 h **(Fig. 6A and B)**. Rather, the marginal decrease in residual enzyme activity observed post-dialysis could be rationalized by enzymatic degradation that occurred during the course of dialysis – as was further confirmed in vehicle control experiments. Furthermore, potassium ferricyanide only marginally restored the metabolic activity of CYP3A4 and CYP3A5 by 1.56 ± 0.01% and 3.05 ± 0.39% respectively after a 30 min preincubation with 25 μM PEM **(Fig. 6C and D)**. Taken together, our results collectively substantiated the irreversible inactivation of CYP3A by PEM.

Spectral Difference Scanning. Consistent with our previous findings, there was an absence of a spectrally detectable peak in the Soret region (448 – 458 nm) – associated with the formation of pseudo-irreversible MIC – when incubation mixtures containing PEM and CYP3A were scanned from 400 to 500 nm at 5 min intervals for

DMD Fast Forward. Published on February 13, 2022 as DOI: 10.1124/dmd.121.000804
This article has not been copyedited and formatted. The final version may differ from this version.

1 h **(Fig. 7A and B)** (Polasek and Miners, 2008). Moreover, tracking the increase in absorbance between 454 nm and the isosbestic point at 490 nm further substantiated the lack of MIC formation with PEM **(Fig. 7C and D)**. On the contrary, previous control experiments involving verapamil (a known pseudoirreversible MIC of CYP3A) produced a discernible peak and a time-dependent increase in absorbance at 454 nm (Tang *et al.*, 2021b)

Cyanide Trapping. A previously described cyanide trapping assay (Argoti *et al.*, 2005) was conducted by fortifying reaction mixtures with the hard nucleophile KCN to uncover iminium ion intermediates of PEM trapped as stable cyano adducts. Remarkably, two peaks consistent with putative PEM-derived cyano conjugates; PEM-C1 (retention time: 6.99 min) and PEM-C2 (retention time: 8.07 min) with $[M+H]^+$ ion at *m/z* of 499 and 513 respectively were detected via a constant NL scan of 27 Da in positive mode but absent in vehicle-containing controls **(Fig. 8A and B)**. The resultant EPI MS/MS spectra acquired further reinforced our postulations that these peaks corresponded to cyano adducts due to its characteristic collision-induced dissociation fragmentation pattern yielding neutral mass loss of 27 Da (corresponding to the loss of HCN) **(Fig. 8C and D)**. To further elucidate the structures of PEM-C1 and PEM-C2, accurate mass measurements were performed. As expected, we were able to recapitulate the nominal mass patterns generated using the QTRAP-MS when the cyano adducts were subjected to accurate mass measurements using the Orbitrap-MS. The proposed elemental composition, theoretical and experimental exact *m/z* and mass accuracy (in both ∆Da and ∆ppm) of the PEM-C1 and PEM-C2 are summarized in **Table 2 and 3**. Additionally, the representative product ion chromatogram, accurate mass MS/MS spectrum and proposed fragmentation pattern of the PEM-derived cyano adducts are depicted in

DMD Fast Forward. Published on February 13, 2022 as DOI: 10.1124/dmd.121.000804
This article has not been copyedited and formatted. The final version may differ from this version.

Fig. 9A – D. Whereas the corresponding Orbitrap-MS data for PEM are illustrated in **Supplemental Fig. 1** and outlined in **Supplemental Table 2**.

Covalent Docking of PEM to CYP3A4 and CYP3A5. As it was previously reported that iminium ion intermediates elicit MBI of P450 via apoprotein alkylation (Orr *et al.*, 2012), we focused our efforts towards identifying susceptible residues in the periphery of the OBS. A total of five lysine (Lys173, Lys208, Lys209, Lys476, and Lys487) and 1 serine (Ser312) residues were identified in the vicinity of the OBS in CYP3A4 as accessible residues that were potentially amenable to covalent adduction by the PEM-derived iminium ion intermediate. Interestingly, our analyses also determined that these aforementioned residues were structurally conserved in CYP3A5. This prompted us to perform covalent docking of PEM on these identified residues in CYP3A4 and CYP3A5. Our findings revealed that for both CYP3A isoforms, the top covalent docking scores were obtained by docking PEM to Ser312. As illustrated in the respective molecular plots **(Fig. 10A and B)**, PEM adducted to Ser312 in both CYP3A isoforms and adopted a binding pose that snuggly occupied the OBS beneath the F-F' loop. On one hand, in CYP3A4, the adduct laid almost parallel to the F-F' loop and completely blocked the opening between the C-terminal and F-F' loop **(Fig. 10A)**. On the other hand, in CYP3A5, the adduct pointed towards the F-F' loop and only partially occluded the opening to the OBS **(Fig. 10B)**. Taken together, these results hinted that PEM covalent adducts possessed a greater propensity to impede substrate access to the catalytic heme in CYP3A4 than in CYP3A5. Consistent with these binding poses, our *in silico* findings also demonstrated that PEM interacted more favorably with Ser312 in CYP3A4 as compared to CYP3A5, as substantiated by their respective docking scores and calculated distances. In particular, the adduction of PEM to Ser312 generated a

DMD Fast Forward. Published on February 13, 2022 as DOI: 10.1124/dmd.121.000804
This article has not been copyedited and formatted. The final version may differ from this version.

more favourable docking score in CYP3A4 (-8.5) than that in CYP3A5 (-7.2). Additionally, the minimum distances between the heavy atoms of the PEM adduct in Ser312 and the F-F' loop was calculated to be considerably shorter in CYP3A4 (2.9 Å) as compared to CYP3A5 (4.2 Å). Conversely, while our covalent docking simulations also revealed that PEM could form adducts with the five conserved lysine residues in both CYP3A isoforms, their binding poses and docking scores were found to be substantially less favorable as compared to that yielded at Ser312 in both isoforms (see **Supplemental Fig. 2 and Supplemental Table 3** for more details). Hence, we are inclined to believe that the covalent adduction at Ser312 is likely to be more pertinent to mechanistically explain both the MBI of CYP3A by PEM as well as to rationalize the observed differences in inactivation potencies between CYP3A4 and CYP3A5.

DMD Fast Forward. Published on February 13, 2022 as DOI: 10.1124/dmd.121.000804
This article has not been copyedited and formatted. The final version may differ from this version.

DISCUSSION

Although it was initially purported that PEM did not pose any metabolism-dependent liabilities (i.e. TDI) due to the absence of GSH-related conjugates in reactive metabolite screens, our findings presented here challenged the veracity of these previous inferences by establishing that PEM exhibited all the classical hallmarks of an archetypal MBI of CYP3A4 and CYP3A5. Following which, we also provided evidence that PEM could be directly and sequentially bioactivated to a reactive iminium ion intermediate that could covalently modify CYP3A and culminate in its MBI.

The K_I and k_{inact} are two important kinetic constants that are intrinsic to an MBI and are reflective of the enzyme-inactivator binding affinities at the molecular level. Consequently, the ratio of k_{inact} to K_I is frequently harnessed in drug discovery to quantitatively assess the *in vitro* inactivation potency of a preclinical drug candidate (Orr *et al.*, 2012). A comparison of the k_{inact}/K_I ratios derived for CYP3A4 revealed that the inactivation potency of PEM was largely comparable with the other FGFR inhibitors **(Table 4)**. Conversely, juxtaposing the k_{inact}/K_I ratios between both CYP3A isoforms for PEM demonstrated that the inactivation of CYP3A4 was approximately 3.5-fold more potent than that in CYP3A5. It was previously established in a high-throughput TDI screen comprising 400 marketed drugs that CYP3A inactivators which possess a k_{obs} value of > 0.020 min^{-1} at a concentration of 10 μM may constitute a potential *in vivo* DDI risk (Zimmerlin *et al.*, 2011). Consistent with the trends observed in the aforementioned k_{inact}/K_I ratios, we estimated that the k_{obs} of CYP3A4 and CYP3A5 at 10 μM were 0.058 min^{-1} and 0.019 min^{-1} respectively. Taken together, it hinted that the inactivation of CYP3A4 by PEM is likely to be more pertinent from a clinical standpoint although it should be noted that at present there

are no reported DDI data pertaining to PEM. At the same time, due to the functional redundancy and overlapping substrate specificities of both CYP3A isoforms, it is plausible that the metabolism of PEM and other co-administered substrates of CYP3A may be preserved due to the less potent inactivation of CYP3A5. However, as the expression levels of CYP3A5 are highly polymorphic across different ethnicities, further studies are vital to mechanistically comprehend the full pharmacogenomic implications of our findings and how they may contribute to interindividual variability in PEM interactions. Additionally, the presence of MBI in PEM may potentially serve as a portentous predictor of reactive metabolite-induced toxicity and therefore warrants closer scrutiny.

Apart from its potency, the efficiency of an MBI can be also quantitatively evaluated by means of its partition ratio, which is defined as the number of inactivator molecules metabolized for every molecule of the enzyme inactivated. Partition ratios ranging from near zero to several thousands have been previously reported and hinges on a number of factors such as the reactivity of the intermediate generated through metabolic activation as well as its relative proximity to the targeted adduct/coordination site, among many others. As highly efficient inactivators are known to possess ratios < 50 (Lim *et al.*, 2005), our data suggests that PEM are relatively efficient MBI of both CYP3A isoforms. Moreover, we also demonstrated that the inactivation of CYP3A by PEM could be attenuated in the presence of testosterone or ketoconazole, thereby implying that inactivation occurred within the enzymatic active site and could be diminished or even abolished by an alternative substrate or direct inhibitor competing for the same binding pocket. On the contrary, such similar protection was not observed in incubation mixtures that were fortified with nucleophilic trapping agents, this implied that reactive intermediate inactivated

the enzyme before it is liberated from the active site and precludes the involvement of ROS in enzyme inactivation.

While our experimental findings collectively supported the MBI of both CYP3A isoforms by PEM, the specific nature of inactivation still remained obfuscated. MIC, which stems from the formation of a coordinate bond between the reactive intermediate and heme ferrous iron are pseudo-irreversible and can be dissociated *in vitro* by means of dialysis or with a strong oxidizing agent which reverts the heme iron back to its ferric state and in doing so displaces the inactivator from the tight-binding complex and restores enzyme catalytic activity. Conversely, enzyme inactivation that arises from covalent alkylation are irreversible and cannot be mitigated by both aforementioned experimental approaches. Moreover, despite sharing ~85% sequence homology between CYP3A4 and CYP3A5, disparate modalities of inactivation have been reported for the same drug (Takakusa *et al.*, 2011; Chan *et al.*, 2012). As PEM possesses a tertiary amine substructure which are known to be capable of undergoing *N*-dealkylation to a reactive nitroso intermediate that can form MIC (Kamel and Harriman, 2013), it is imperative to individually delineate the nature of inactivation of both CYP3A isoforms by PEM. Here, our findings demonstrated that the loss of CYP3A activity is irrevocable and could not be recovered after dialysis. Similarly, the addition of potassium ferricyanide also did not restore enzyme activity by more than 20% – which is the predetermined threshold for MIC-forming inactivators (Watanabe *et al.*, 2007). Finally, the lack of the diagnostic Soret peak in our spectral analyses further cemented our postulations that the inactivation of CYP3A by PEM was not mechanistically tied to the formation of pseudo-irreversible MIC but rather via irreversible covalent alkylation.

DMD Fast Forward. Published on February 13, 2022 as DOI: 10.1124/dmd.121.000804
This article has not been copyedited and formatted. The final version may differ from this version.

Consistent with a previous report by the drug's manufacturer (Wu *et al.*, 2021), we also did not manage to evince any GSH conjugates in reactive metabolite screens performed in human liver microsomes or rhCYP3A4/5 (data not shown). This was rather peculiar as a core tenet underscoring MBI of P450 is the generation of chemically reactive metabolite(s) as the molecular-initiating event. Consequently, we surmised that the reactive intermediate of PEM implicated in the covalent modification of CYP3A may be a hard electrophile which cannot be efficiently trapped by GSH. Notably, one susceptible chemical motif in PEM that may be metabolically activated to such species is its distal morpholine ring which are amenable to undergo oxidative bioactivation to an iminium ion intermediate (Peterlin Masic, 2011; Bolleddula *et al.*, 2014). These reactive species generated *in situ* can then be readily trapped as stable cyano adducts by KCN and detected via NL of 27 Da in positive ESI mode (Argoti *et al.*, 2005). Our postulations were indeed proven to be correct when we detected two putative adducts of PEM in our cyano trapping assays. Moreover, the successful recapitulation of the nominal mass EPI spectral peaks for both adducts in our high-resolution Orbitrap-MS along with mass accuracies well below the mass tolerance threshold of 5 ppm allowed us to confidently ascertain that the direct and sequential bioactivation of PEM and its major *O*-desmethylated metabolite arose from P450-catalyzed hydroxylation at the α-carbon of the morpholine nitrogen to an unstable carbinolamine that can undergo further dehydration to form the reactive iminium ion intermediate. Thereafter, the adduction of these hard electrophiles to cyanide yields the conjugates PEM-C1 and PEM-C2 respectively **(Fig. 11)**.

Although the formation of reactive iminium ions from cyclic amines-containing compounds may occasionally be desirable – as evident in methoxy-4-morpholinyl

DMD Fast Forward. Published on February 13, 2022 as DOI: 10.1124/dmd.121.000804
This article has not been copyedited and formatted. The final version may differ from this version.

doxorubicin where the iminium species potentiates its antineoplastic activity by facilitating DNA alkylation (Quintieri *et al.*, 2005), more often than not, they are deleterious to its pharmacology (Kalgutkar, 2017). A well-established paradigm of this phenomenon can be gleaned from the withdrawn cannabinoid receptor 1 antagonist rimonabant. Studies have shown that rimonabant was bioactivated by CYP3A4 to an iminium intermediate which resulted in extensive covalent binding to microsomal protein and cytotoxicity in human hepatocytes and SV40-THLE cells overexpressing CYP3A4 (Foster *et al.*, 2012). More importantly, rimonabant was also discovered to incite TDI of CYP3A4 (Bergström *et al.*, 2011). Consequently, we believe that the iminium species generated from PEM could likewise covalently modify CYP3A and culminate in its MBI. As such, covalent docking was conducted to elucidate plausible molecular determinants underpinning the MBI of CYP3A by PEM. Our findings collectively hinted that the salient discrepancies in MBI potencies between the CYP3A isoforms might be alluded to the propensity for PEM to interact more favorably with a conserved serine residue in position 312 of CYP3A4 as compared to CYP3A5. The involvement of serine here is not unexpected as the implicated iminium ion species is a hard electrophile and will preferentially react with a nucleophile of comparable ‘hardness’ such as the hydroxyl groups of serine residues (LoPachin and DeCaprio, 2005). Additionally, the possibility of this serine residue being implicated in its MBI is further reinforced by a recent study which identified Ser312 in CYP3A4 as an important binding site residue implicated in ligand inhibitory interactions (Kiani *et al.*, 2019).

In conclusion, our findings established that PEM is an archetypal MBI of CYP3A. Furthermore, we also illuminated the direct and sequential bioactivation pathways of PEM and its major *O*-desmethylated metabolite to reactive iminium ion species

DMD Fast Forward. Published on February 13, 2022 as DOI: 10.1124/dmd.121.000804
This article has not been copyedited and formatted. The final version may differ from this version.

which are likely to be implicated in the irreversible covalent modification of CYP3A. Due to the profound pharmacokinetic and toxicological liabilities associated with hard electrophiles, we advocate that reactive metabolite screens should routinely monitor for both types of soft and hard electrophilic species.

DMD Fast Forward. Published on February 13, 2022 as DOI: 10.1124/dmd.121.000804
This article has not been copyedited and formatted. The final version may differ from this version.

AUTHORSHIP CONTRIBUTIONS

Participated in research design:	Tang, Wei, Verma, Fan, Chan
Conducted experiments:	Tang, Wei, Verma, Koh
Contributed new reagents or analytical tools:	Koh, Zhou, Fan
Performed data analysis:	Tang, Wei, Verma, Fan, Chan
Wrote or contributed to the writing of the manuscript:	Tang, Wei, Verma, Fan, Chan

DMD Fast Forward. Published on February 13, 2022 as DOI: 10.1124/dmd.121.000804
This article has not been copyedited and formatted. The final version may differ from this version.

BIBLIOGRAPHY

Argoti D, Liang L, Conteh A, Chen L, Bershas D, Yu CP, Vouros P, and Yang E (2005) Cyanide trapping of iminium ion reactive intermediates followed by detection and structure identification using liquid chromatography-tandem mass spectrometry (LC-MS/MS). *Chem Res Toxicol* **18**:1537–1544.

Babina IS, and Turner NC (2017) Advances and challenges in targeting FGFR signalling in cancer. *Nat Rev Cancer 2017 175* **17**:318–332, Nature Publishing Group.

Bergström MA, Isin EM, Castagnoli N, and Milne CE (2011) Bioactivation Pathways of the Cannabinoid Receptor 1 Antagonist Rimonabant. *Drug Metab Dispos* **39**:1823–1832, American Society for Pharmacology and Experimental Therapeutics.

Bjornsson TD, Callaghan JT, Einolf HJ, Fischer V, Gan L, Grimm S, Kao J, King SP, Miwa G, Ni L, Kumar G, McLeod J, Obach RS, Roberts S, Roe A, Shah A, Snikeris F, Sullivan JT, Tweedie D, Vega JM, Walsh J, and Wrighton SA (2003) The conduct of in vitro and in vivo drug-drug interaction studies: A Pharmaceutical Research and Manufacturers of America (PhRMA) perspective. *Drug Metab Dispos* **31**:815–832.

Bolleddula J, Dement K, Driscoll JP, Worboys P, Brassil PJ, and Bourdet DL (2014) Biotransformation and bioactivation reactions of alicyclic amines in drug molecules. *Drug Metab Rev* **46**:379–419.

Chae YK, Ranganath K, Hammerman PS, Vaklavas C, Mohindra N, Kalyan A, Matsangou M, Costa R, Carneiro B, Villaflor VM, Cristofanilli M, and Giles FJ (2017) Inhibition of the fibroblast growth factor receptor (FGFR) pathway: The current landscape and barriers to clinical application. *Oncotarget* **8**:16052–16074, Impact Journals LLC.

Chan ECY, New LS, Chua TB, Yap CW, Ho HK, and Nelson SD (2012) Interaction of lapatinib with cytochrome P450 3A5. *Drug Metab Dispos* **40**:1414–1422.

Dienstmann R, Rodon J, Prat A, Perez-Garcia J, Adamo B, Felip E, Cortes J, Iafrate AJ, Nuciforo P, and Tabernero J (2014) Genomic aberrations in the FGFR pathway: Opportunities for targeted therapies in solid tumors. *Ann Oncol* **25**:552–563.

Foster AJ, Prime LH, Gustafsson F, Temesi DG, Isin EM, Midlöv J, Neal Castagnoli J, and Kenna JG (2012) Bioactivation of the Cannabinoid Receptor Antagonist Rimonabant to a Cytotoxic Iminium Ion Metabolite. *Chem Res Toxicol* **26**:124–135, American Chemical Society.

Friesner RA, Banks JL, Murphy RB, Halgren TA, Klicic JJ, Mainz DT, Repasky MP, Knoll EH, Shelley M, Perry JK, Shaw DE, Francis P, and Shenkin PS (2004) Glide: A New Approach for Rapid, Accurate Docking and Scoring. 1. Method and Assessment of Docking Accuracy. *ACS Publ* **47**:1739–1749.

Ghedini GC, Ronca R, Presta M, and Giacomini A (2018) Future applications of

FGF/FGFR inhibitors in cancer. *https://doi.org/101080/1473714020181491795* **18**:861–872, Taylor & Francis.

Guengerich FP (2001) Common and Uncommon Cytochrome P450 Reactions Related to Metabolism and Chemical Toxicity. *Chem Res Toxicol* **14**:611–650, American Chemical Society .

Ho HK, Chan JCY, Hardy KD, and Chan ECY (2015) Mechanism-based inactivation of CYP450 enzymes: A case study of lapatinib. *Drug Metab Rev* **47**:21–28.

Hoy SM (2020) Pemigatinib: First Approval. *Drugs* **80**:923–929, Adis.

Ji T, Rockich K, Epstein N, Overholt H, Wang P, Chen X, Punwani N, and Yeleswaram S (2021) Evaluation of drug-drug interactions of pemigatinib in healthy participants. *Eur J Clin Pharmacol* **77**:1887–1897, Springer.

Kalgutkar AS (2017) Liabilities associated with the formation of “hard” electrophiles in reactive metabolite trapping screens. *Chem Res Toxicol* **30**:220–238.

Kamel A, and Harriman S (2013) Inhibition of cytochrome P450 enzymes and biochemical aspects of mechanism-based inactivation (MBI). *Drug Discov Today Technol* **10**:e177–e189, Elsevier Ltd.

Kiani YS, Ranaghan KE, Jabeen I, and Mulholland AJ (2019) Molecular Dynamics Simulation Framework to Probe the Binding Hypothesis of CYP3A4 Inhibitors. *Int J Mol Sci 2019, Vol 20, Page 4468* **20**:4468, Multidisciplinary Digital Publishing Institute.

Kim S, Chen J, Cheng T, Gindulyte A, He J, He S, Li Q, Shoemaker BA, Thiessen PA, Yu B, Zaslavsky L, Zhang J, and Bolton EE (2019) PubChem 2019 update: improved access to chemical data. *Nucleic Acids Res* **47**:D1102–D1109, Oxford Academic.

Kitz R, and Wilson IB (1962) Esters of methanesulfonic acid as irreversible inhibitors of acetylcholinesterase. *J Biol Chem* **237**:3245–3249.

Lim HK, Duczak N, Brougham L, Elliot M, Patel K, and Chan K (2005) Automated screening with confirmation of mechanism-based inactivation of CYP3A4, CYP2C9, CYP2C19, CYP2D6, and CYP1A2 in pooled human liver microsomes. *Drug Metab Dispos* **33**:1211–1219.

Liu PCC, Koblish H, Wu L, Bowman K, Diamond S, DiMatteo D, Zhang Y, Hansbury M, Rupar M, Wen X, Collier P, Feldman P, Klabe R, Burke KA, Soloviev M, Gardiner C, He X, Volgina A, Covington M, Ruggeri B, Wynn R, Burn TC, Scherle P, Yeleswaram S, Yao W, Huber R, and Hollis G (2020) INCB054828 (pemigatinib), a potent and selective inhibitor of fibroblast growth factor receptors 1, 2, and 3, displays activity against genetically defined tumor models. *PLoS One* **15**:1–16.

LoPachin RM, and DeCaprio AP (2005) Protein adduct formation as a molecular mechanism in neurotoxicity. *Toxicol Sci* **86**:214–225.

Markham A (2019) Erdafitinib: First Global Approval. *Drugs* **79**:1017–1021, Springer International Publishing.

Masubuchi Y, and Horie T (2007) Toxicological significance of mechanism-based inactivation of cytochrome P450 enzymes by drugs, Taylor & Francis.

Orr STM, Ripp SL, Ballard TE, Henderson JL, Scott DO, Obach RS, Sun H, and Kalgutkar AS (2012) Mechanism-based inactivation (MBI) of cytochrome P450 enzymes: Structure-activity relationships and discovery strategies to mitigate drug-drug interaction risks. *J Med Chem* **55**:4896–4933.

Pearson RG (1963) Hard and Soft Acids and Bases. *J Am Chem Soc* **85**:3533–3539, American Chemical Society .

Peterlin Masic L (2011) Role of Cyclic Tertiary Amine Bioactivation to Reactive Iminium Species: Structure Toxicity Relationship. *Curr Drug Metab* **12**:35–50.

Polasek TM, and Miners JO (2008) Time-dependent inhibition of human drug metabolizing cytochromes P450 by tricyclic antidepressants. *Br J Clin Pharmacol* **65**:87–97.

Quintieri L, Geroni C, Fantin M, Battaglia R, Rosato A, Speed W, Zanovello P, and Floreani M (2005) Formation and Antitumor Activity of PNU-159682, A Major Metabolite of Nemorubicin in Human Liver Microsomes. *Clin Cancer Res* **11**:1608–1617, American Association for Cancer Research.

Silverman RB (1995) Mechanism-based enzyme inactivators. *Methods Enzymol* **249**:240–283.

Stephens C, Andrade RJ, and Lucena MI (2014) Mechanisms of drug-induced liver injury.

Takakusa H, Wahlin MD, Zhao C, Hanson KL, New LS, Chan ECY, and Nelson SD (2011) Metabolic intermediate complex formation of human cytochrome P450 3A4 by lapatinib. *Drug Metab Dispos* **39**:1022–1030, American Society for Pharmacology and Experimental Therapeutics.

Tang LWT, Teng Jian Wei, Koh SK, Zhou L, Go ML, and Chan ECY (2021a) Mechanism-Based Inactivation of Cytochrome P450 3A4 and 3A5 by the Fibroblast Growth Factor Receptor Inhibitor Erdafitinib. *Chem Res Toxicol* **34**:1800–1813.

Tang LWT, Teng Jian Wei, Verma RK, Koh SK, Zhou L, Go ML, Fan H, and Chan ECY (2021b) Infigratinib Is a Reversible Inhibitor and Mechanism-Based Inactivator of Cytochrome P450 3A4. *Drug Metab Dispos* **49**:856–868, American Society for Pharmacology and Experimental Therapeutics.

Tang LWT, Verma RK, Fan H, and Chan ECY (2021c) Mechanism-Based Inactivation of Cytochrome P450 3A4 by Benzbromarone. *Mol Pharmacol* **99**:266–276, American Society for Pharmacology & Experimental Therapeutics (ASPET).

Tang LWT, Verma RK, Yong RP, Li X, Wang L, Lin Q, Fan H, and Chan ECY (2021d) Differential Reversible and Irreversible Interactions between Benzbromarone and Human Cytochrome P450s 3A4 and 3A5. *Mol Pharmacol* **100**:224–236.

Turner N, and Grose R (2010) Fibroblast growth factor signalling: From development to cancer, Nat Rev Cancer.

Watanabe A, Nakamura K, Okudaira N, Okazaki O, and Sudo KI (2007) Risk assessment for drug-drug interaction caused by metabolism-based inhibition of CYP3A using automated in vitro assay systems and its application in the early drug discovery process. *Drug Metab Dispos* **35**:1232–1238.

Wu L, Zhang C, He C, Qian D, Lu L, Sun Y, Xu M, Zhuo J, Liu PCC, Klabe R, Wynn R, Covington M, Gallagher K, Leffet L, Bowman K, Diamond S, Koblish H, Zhang Y, Soloviev M, Hollis G, Burn TC, Scherle P, Yeleswaram S, Huber R, and Yao W (2021) Discovery of Pemigatinib: A Potent and Selective Fibroblast Growth Factor Receptor (FGFR) Inhibitor. *J Med Chem* **64**:10666–10679.

Zanger UM, and Schwab M (2013) Cytochrome P450 enzymes in drug metabolism: Regulation of gene expression, enzyme activities, and impact of genetic variation, Pergamon.

Zanger UM, Turpeinen M, Klein K, and Schwab M (2008) Functional pharmacogenetics/genomics of human cytochromes P450 involved in drug biotransformation.

Zhu K, Borrelli KW, Greenwood JR, Day T, Abel R, Farid RS, and Harder E (2014) Docking covalent inhibitors: A parameter free approach to pose prediction and scoring. *J Chem Inf Model* **54**:1932–1940, American Chemical Society.

Zimmerlin A, Trunzer M, and Faller B (2011) CYP3A Time-Dependent Inhibition Risk Assessment Validated with 400 Reference Drugs. *Drug Metab Dispos* **39**:1039–1046, American Society for Pharmacology and Experimental Therapeutics.

DMD Fast Forward. Published on February 13, 2022 as DOI: 10.1124/dmd.121.000804
This article has not been copyedited and formatted. The final version may differ from this version.

FOOTNOTES

This work was supported by the Agency for Science, Technology and Research (A*STAR) Industry Alignment Fund – Pre-Positioning (IAF-PP) [Grant H18/01/a0/C14] and the Joseph Lim Boon Tiong Urology Cancer Research Initiative [Grant: R-148-000-302-720] to E.C.Y.C. L.W.T.T is supported by the National University of Singapore (NUS) President's Graduate Fellowship (PGF).

The authors declare that they have no conflicts of interest with the contents of this article.

DMD Fast Forward. Published on February 13, 2022 as DOI: 10.1124/dmd.121.000804
This article has not been copyedited and formatted. The final version may differ from this version.

FIGURE LEGENDS

Fig. 1. Chemical structure of (A) pemigatinib (PEM) and its (B) major *O*-desmethylated metabolite

Fig. 2. Substrate depletion of PEM by CYP3A. Percentage of PEM remaining against time in the presence of (A) CYP3A4 and (B) CYP3A5 plotted on a linear scale and the corresponding substrate depletion graphs of PEM in the presence of (C) CYP3A4 and (D) CYP3A5 as plotted on a semi-natural logarithmic scale. Each point in (A to D) represents the mean and S.D. of triplicate experiments.

Fig. 3. Time- and concentration-dependent inactivation of (A) CYP3A4 and (D) CYP3A5 by PEM using rivaroxaban as probe substrate. Nonlinear regression of observed first-order inactivation rate constants (k_{obs}) versus PEM concentration yielded K_I and k_{inact} values of (B) 8.69 ± 1.62 μM and 0.108 ± 0.008 min^{-1} for CYP3A4 and (E) 11.95 ± 4.41 μM and 0.042 ± 0.007 min^{-1} for CYP3A5. Cofactor NADPH-dependent inactivation of (C) CYP3A4 and (F) CYP3A5 by PEM. Each point in (A, C, D and F) represents the mean and S.D. of triplicate experiments.

Fig. 4. Partition ratio for the inactivation of (A) CYP3A4 and (B) CYP3A5 by PEM, determined by extrapolating the intercept of the linear regression line at lower ratios and the straight line for the high ratios to the x-axis, was estimated to be 44 and 47, respectively. Each point in (A and B) represents the mean and S.D. of triplicate experiments.

Fig. 5. Inactivation of CYP3A4 and CYP3A5 was attenuated in the presence of (A and D) an alternative CYP3A substrate testosterone and (B and E) a direct CYP3A inhibitor ketoconazole (KTC). (C and F) Conversely, the presence of either GSH,

KCN or catalase did not protect against enzymatic inactivation. Each point in (A to F) represents the mean and S.D. of triplicate experiments.

Fig. 6. Percentage activity of (A) CYP3A4 and (B) CYP3A5 remaining did not increase after extensive dialysis at 4°C for 4 h. Similarly, potassium ferricyanide (KFC) only restored the metabolic activity of (C) CYP3A4 and (D) CYP3A5 by a modest 1.56 ± 0.01% and 3.05 ± 0.39% after a 30 min incubation with 25 μM PEM. Results from all four graphs depict the mean and S.D. of three independent experiments conducted in triplicates.

Fig. 7. Spectral difference measured over 60 min failed to elicit a Soret peak in the absorbance ranges of 448 – 458 nm for (A) CYP3A4 and (B) CYP3A5 incubated with 25 μM PEM. Similarly, a comparison of the absorbance at the reference of 454 nm against the isosbestic point at 490 nm failed to demonstrate an increase in the extent of MIC formation over time in (C) CYP3A4 and (D) CYP3A5 incubation mixtures.

Fig. 8. Total ion chromatogram for constant NL scan of 27 Da in positive ESI mode of (A) vehicle and (B) pemigatinib incubations in the cyanide trapping assay. Notably, two peaks corresponding to PEM-derived cyano adducts PEM-C1 (retention time: 6.99 min) and PEM-C2 (retention time 8.07 min) were apparent in incubation mixtures containing PEM. Representative EPI MS/MS spectra of (C) PEM-C1 (*m/z* 499) and (D) PEM-C2 (*m/z* 513) formed *in situ* in the cyanide trapping assay.

Fig. 9. (A) Representative product ion chromatogram of (A) PEM-C1 (retention time: 6.79 min) and (B) PEM-C2 (retention time: 7.84 min). Proposed accurate mass fragmentation pattern of (C) PEM-C1 and (D) PEM-C2. The exact mass MS/MS spectra depict the experimental *m/z* values whereas the chemical structures (inset)

DMD Fast Forward. Published on February 13, 2022 as DOI: 10.1124/dmd.121.000804
This article has not been copyedited and formatted. The final version may differ from this version.

illustrate the theoretical accurate *m/z* values of the parent and product ions of the cyano adducts as outlined in Table 2 and 3 using a mass tolerance of 5 ppm.

Fig. 10. Proposed covalent adduction of PEM to CYP3A4 and CYP3A5. Molecular plots illustrating the top scored binding poses for PEM adducts at (A) Ser312 of CYP3A4 (PDB ID: 4K9V) with a docking score of -8.5 and a minimum distance between the heavy atoms of PEM and the F-F' loop of 2.9 Å and (B) Ser312 of CYP3A5 (cluster 13) with a docking score of -7.2 and a minimum distance between the heavy atoms of PEM and the F-F' loop of 4.2 Å. Color code: F-F' loop, orange; C terminal loop, blue; heme moiety, green; PEM, pink stick with white surface.

Fig. 11. Proposed bioactivation pathways of PEM and its *O*-desmethylated metabolite by CYP3A.

DMD Fast Forward. Published on February 13, 2022 as DOI: 10.1124/dmd.121.000804
This article has not been copyedited and formatted. The final version may differ from this version.

Table 1. CYP3A inactivation kinetic parameters for PEM derived using morpholinone hydroxylation of rivaroxaban as a surrogate marker of residual CYP3A activity. Data are presented as means ± S.D.

P450 Isoform	**K_I (μM)**	**k_{inact} (min^{-1})**	**k_{inact}/K_I ($min^{-1}mM^{-1}$)**	**$t_{1/2}$ (min)**	**Partition Ratio**
CYP3A4	8.69 ± 1.62	0.108 ± 0.008	12.4	6.4	~44
CYP3A5	11.95 ± 4.41	0.042 ± 0.007	3.5	16.5	~47

DMD Fast Forward. Published on February 13, 2022 as DOI: 10.1124/dmd.121.000804
This article has not been copyedited and formatted. The final version may differ from this version.

Table 2. Accurate mass measurement of the parent and product ions of PEM-derived cyano adduct PEM-C1 using a mass tolerance of 5 ppm.

Proposed Elemental Composition	**Theoretical *m/z***	**Experimental *m/z***	**Mass Accuracy**	
			∆Da	**∆ppm**
$C_{24}H_{25}O_4N_6F_2$	499.1900	499.1921	0.0021	4.2
$C_{23}H_{24}O_4N_5F_2$	472.1791	472.1793	0.0002	0.4
$C_{19}H_{17}O_3N_4F_2$	387.1263	387.1267	0.0004	1.0

DMD Fast Forward. Published on February 13, 2022 as DOI: 10.1124/dmd.121.000804
This article has not been copyedited and formatted. The final version may differ from this version.

Table 3. Accurate mass measurement of the parent and product ions of PEM-derived cyano adduct PEM-C2 using a mass tolerance of 5 ppm.

Proposed Elemental Composition	**Theoretical *m/z***	**Experimental *m/z***	**Mass Accuracy**	
			∆Da	**∆ppm**
$C_{25}H_{27}O_4N_6F_2$	513.2056	513.2032	-0.0024	-4.7
$C_{24}H_{26}O_4N_5F_2$	486.1947	486.1950	0.0003	0.6
$C_{20}H_{19}O_3N_4F_2$	401.1420	401.1423	0.0003	0.7

DMD Fast Forward. Published on February 13, 2022 as DOI: 10.1124/dmd.121.000804
This article has not been copyedited and formatted. The final version may differ from this version.

Table 4. Comparison of the CYP3A4 enzyme inactivation kinetic parameters between PEM and other FGFR inhibitors using rivaroxaban hydroxylation as a marker reaction of CYP3A activity.

Compound	K_I **(μM)**	k_{inact} **(min^{-1})**	k_{inact}/K_I **(min^{-1} mM^{-1})**	**Reference**
PEM	8.69	0.108	12.4	
Erdafitinib	4.01	0.120	29.9	(Tang *et al.*, 2021a)
Infigratinib	4.17	0.068	16.4	(Tang *et al.*, 2021b)

Figure 1

A

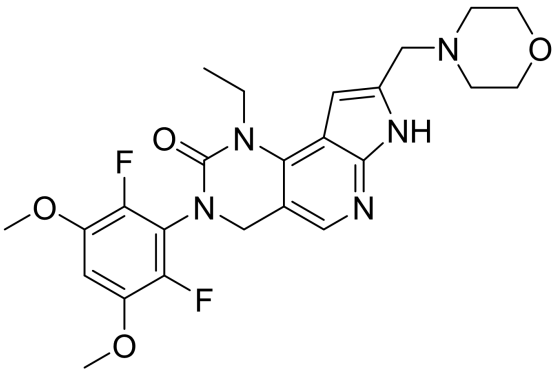

Pemigatinib

B

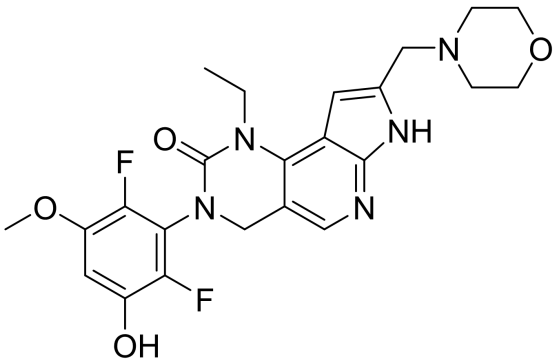

***O*-desmethyl pemigatinib**

Figure 2

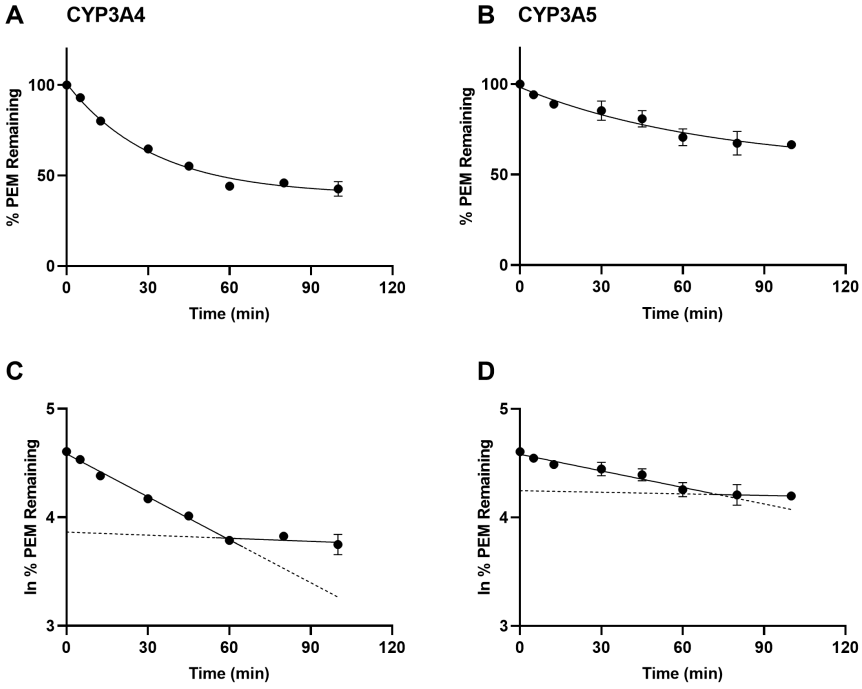

Figure 3

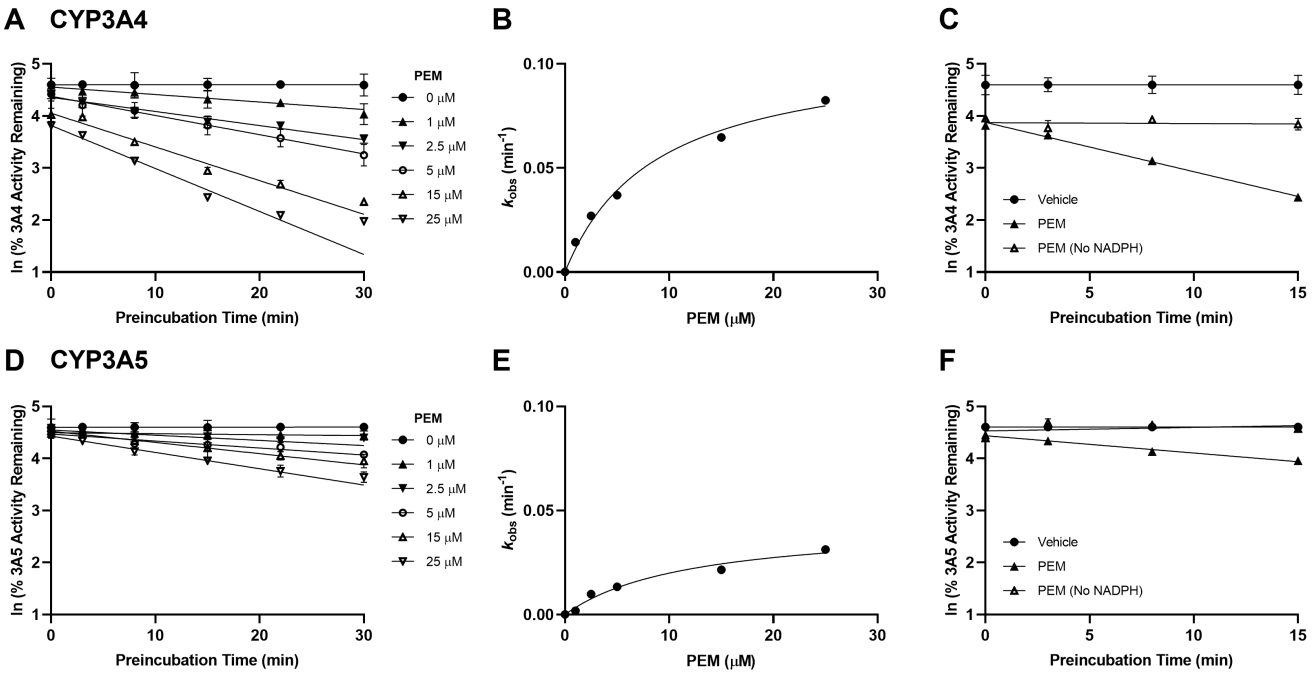

Figure 4

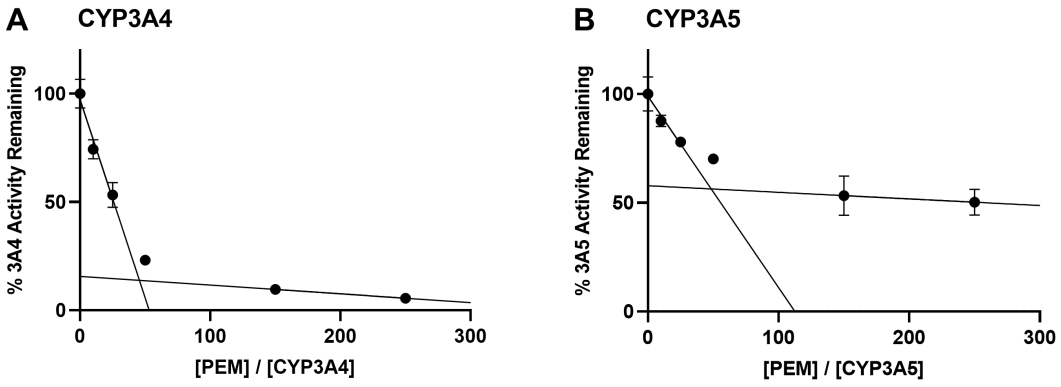

Figure 5

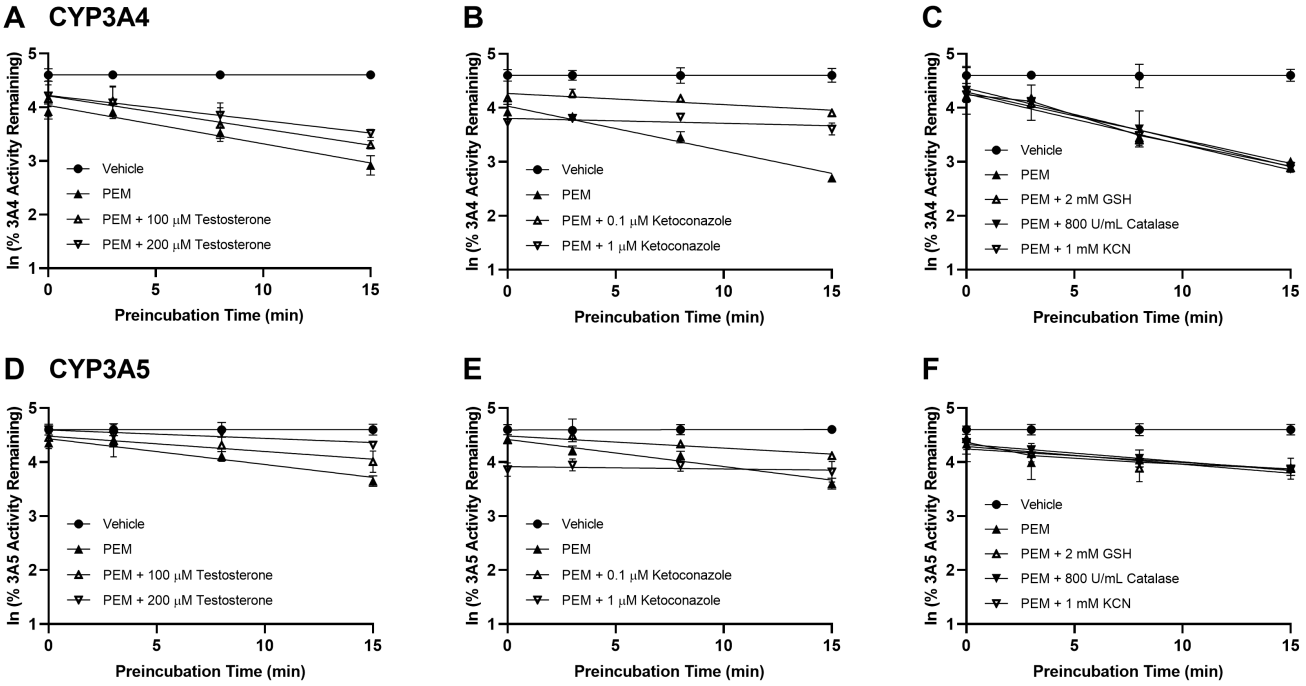

Figure 6

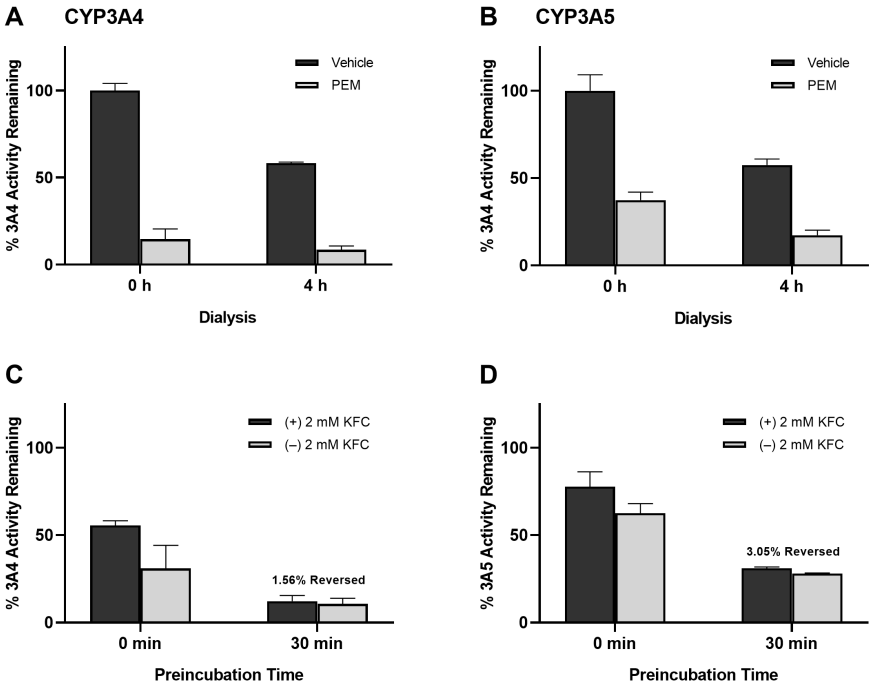

Figure 7

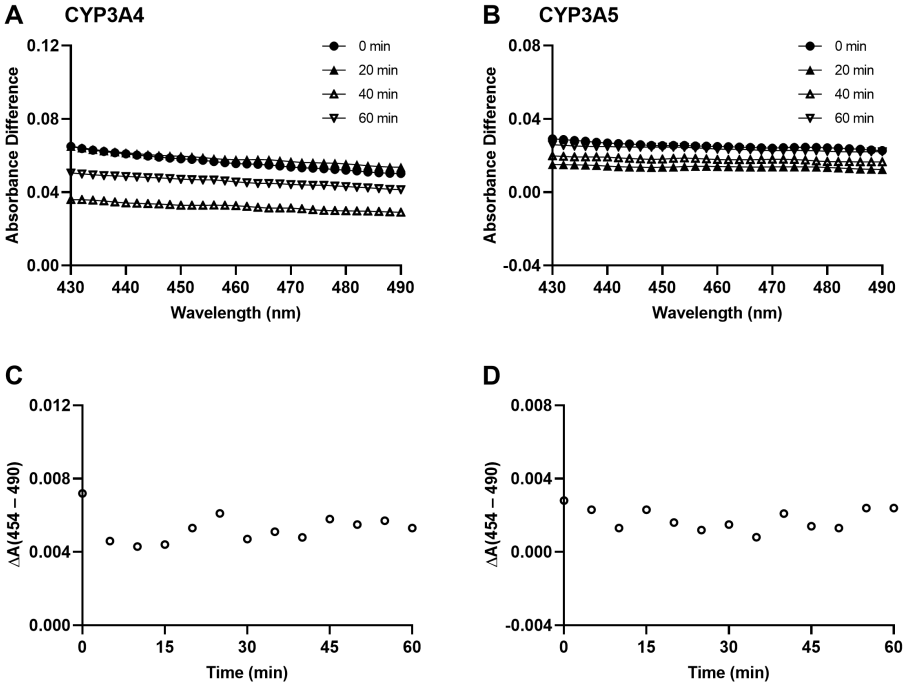

Figure 8

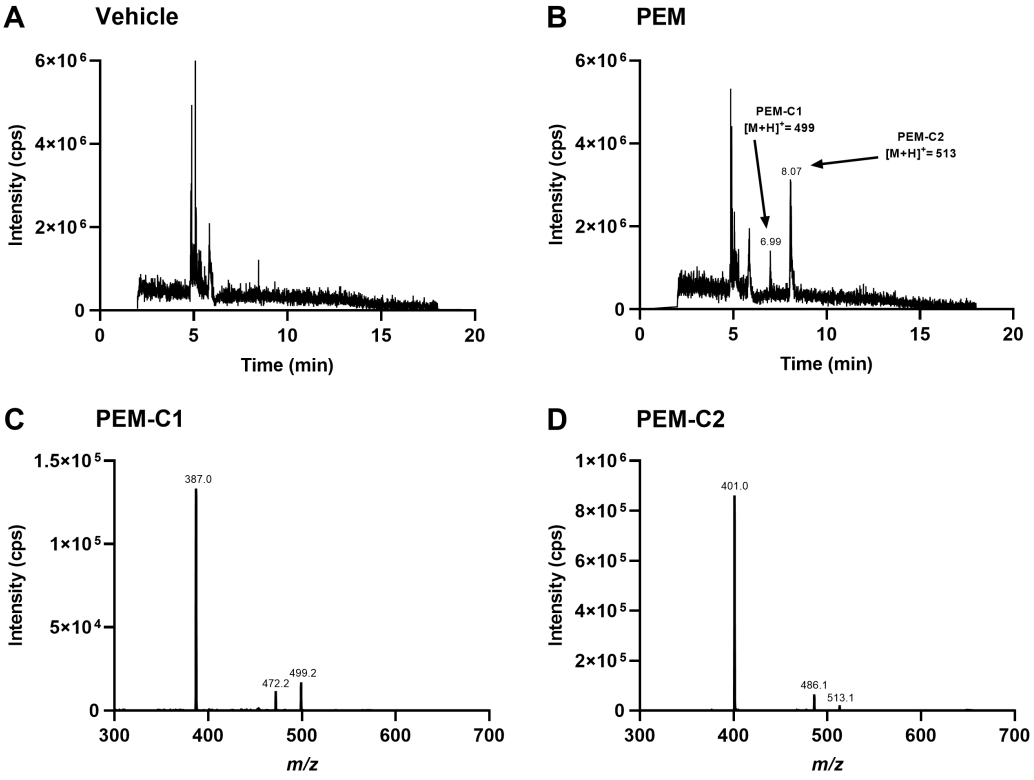

Figure 9

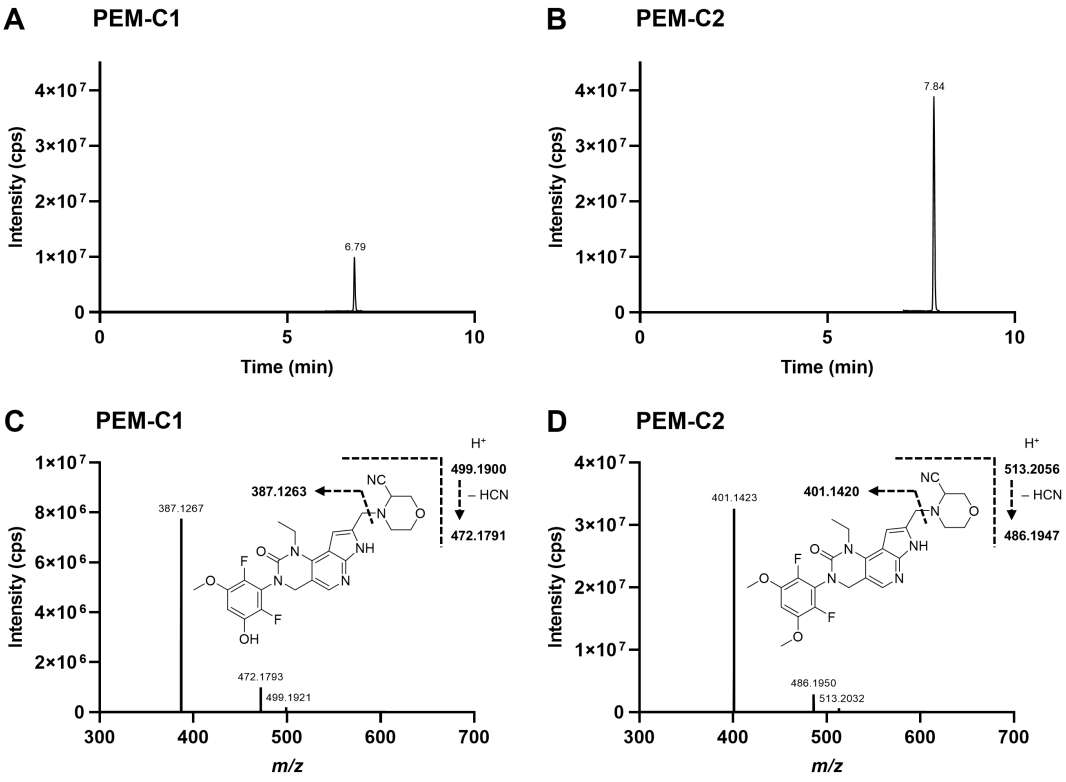

Figure 10

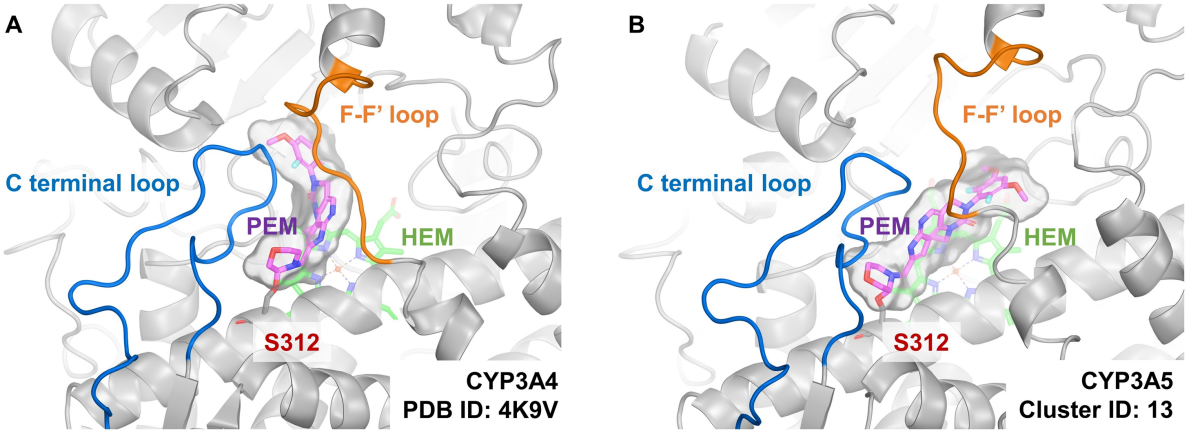

Figure 11